Published April 13, 2017

Original Research

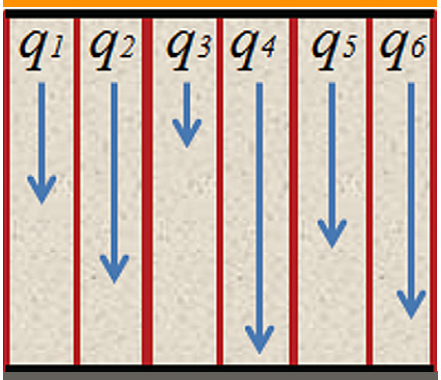

Critical Role of Preferential Flow in Field-Scale Pathogen Transport and Retention

Scott A. Bradford,* Feike J. Leij, Jack Schijven, and Saeed Torkzaban

A stream tube model was applied to simulate pathogen transport and fate in the subsurface at the field scale. Local-scale transport within each stream tube was described deterministically using analytic solutions for pathogen transport and fate in a uniform or dual-permeability porous medium. Important pathogen transport and fate processes that were accounted for in an individual stream tube included: advection, dispersion, reversible and irreversible retention, and decay in the liquid and solid phases. The velocity in a stream tube was related to a median grain size using the Kozeny–Carman equation, and filtration theory was used to predict the dependence of retention on physicochemical factors. The field-scale velocity distribution was described using a unimodal or bimodal lognormal probability density function (PDF). The bimodal lognormal PDF was used in conjunction with the dual-permeability model to account for exchange between slow and fast velocity domains. The mean and variance of the field-scale concentrations were calculated from local-scale stream tube information. The setback distance to achieve a selected risk of infection was determined from the modeled concentrations and a simplified risk assessment approach. Simulation results demonstrate that field-scale pathogen transport and setback distance were very sensitive to velocity distribution characteristics. Early breakthrough, higher peak concentrations, and larger setback distances were associated with faster stream tubes that had little retention, whereas the opposite trends were associated with slower stream tubes. The relative importance of faster stream tubes increased under physicochemical conditions that enhanced retention.

Core Ideas

- A stochastic stream tube model was extended to simulate field-scale pathogen transport and fate.
- Single- or dual-permeability versions of the model were developed that included filtration theory.
- Pathogen transport and fate are highly dependent on the field-scale velocity distribution.
- Physical nonequilibrium effects are coupled with retention, the velocity PDF, and exchange.

Abbreviations: BTC, breakthrough curve; CFT, colloid filtration theory; DPM, dual-permeability model; PDF, probability density function; RP, retention profile; SSTM, stochastic stream tube model; SWI, solid–water interface; UM, uniform model.

S.A. Bradford, USDA–ARS, US Salinity Lab., Riverside, CA 92507; F.J. Leij, Dep. of Civil Engineering and Construction Engineering Management, California State Univ., Long Beach, CA 90840-5101; J. Schijven, Quantitative Microbial Water Safety, Environmental Hydrogeology Group, Faculty of Geosciences, Utrecht Univ., 3508 TC Utrecht, the Netherlands; S. Torkzaban, CSIRO Land and Water, Glen Osmond, SA 5064, Australia. *Corresponding author (Scott.Bradford@ars.usda.gov).

Vadose Zone J.
doi:10.2136/vzj2016.12.0127
Received 8 Dec. 2016.
Accepted 24 Feb. 2017.

Vol. 16, Iss. 4, 2017

Surveys of shallow and deep groundwater wells frequently find the presence of indicator and/or pathogenic microorganisms (World Health Organization, 2011; Borchardt et al., 2007; Li et al., 2015). Contamination of groundwater by pathogens has been linked to waterborne and foodborne disease outbreaks (Steele and Odumeru, 2004; Craun et al., 2010; Borchardt et al., 2011; UN World Water Assessment Program, 2015) that pose a serious risk to public health (Embrey and Runkle, 2006; World Health Organization, 2011; Bradford et al., 2013). Riverbank filtration, sand filtration, and natural and managed aquifer recharge are frequently relied on to remove pathogenic microorganisms from surface water and wastewater supplies that are eventually used for drinking water or irrigation water for fresh produce (Schijven and Hassanizadeh, 2000; Ray et al., 2003; Kazner et al., 2012). An understanding of the processes and factors that influence pathogen transport and fate in porous media is therefore needed to accurately assess the risks of contamination and to produce safe drinking water (Schijven et al., 2006, 2011).

Most microbial transport studies have been conducted using homogeneous, repacked soil columns (Ginn et al., 2002; Harvey and Harms, 2002; Jin and Flury, 2002; Rockhold et al., 2004; Unc and Goss, 2004; Foppen and Schijven, 2006; Bradford et al., 2013). Results have typically been analyzed using models that consider advective–dispersive transport

and first-order microbial retention and release. The pore-water velocity (v) controls the advective transport and residence time of microbes in porous media. Colloid filtration theory (CFT) has often been used to predict the retention rate coefficient (k_{sw}) under saturated conditions (Yao et al., 1971). Colloid filtration theory predicts that k_{sw} is a function of the single-collector efficiency (η), the sticking efficiency (α), and v. The value of η accounts for the mass flux of microbes to the collector surface via diffusion, interception, and gravitational sedimentation. Correlation equations have been developed from pore-scale simulations of colloid transport in simplified grain geometries to predict η as a function of v, the median grain size (d_{50}), the microbe size (d_m), and the microbe density (e.g., Tufenkji and Elimelech, 2004; Messina et al., 2015). Colloid filtration theory originally assumed that α depended only on the adhesive interaction between the microbe and solid, and was independent of v (Elimelech et al., 1998). Experimental results in repacked columns and CFT predictions typically indicate limited potential for microorganism transport in soil and aquifer sediments, but greater microbial transport is expected with a decrease in α and an increase in d_{50} and v (Schijven and Hassanizadeh, 2000; Gupta et al., 2009; Kim et al., 2010; Bradford et al., 2013). Spatial variations in subsurface grain size and water velocity are therefore expected to be critical factors in determining pathogen transport.

Experiments in undisturbed (intact) soil columns, lysimeters, tile drained fields, and the field indicate that colloids and microorganisms can travel much deeper and faster than would be predicted based on the results from repacked column studies (Taylor et al., 2004; Pang, 2009; Sinreich and Flynn, 2011; Bradford et al., 2013; Arnaud et al., 2015; Flynn et al., 2015). Drastic spatial and temporal variability in water flow occurs in natural, heterogeneous subsurface environments because the local hydraulic conductivity can vary by orders of magnitude across a few centimeters (LeBlanc et al., 1991), and it changes in a nonlinear fashion with the water saturation (e.g., Mualem, 1976; van Genuchten, 1980; Schaap et al., 2001). In contrast, the water flow field is relatively uniform and well defined in homogeneous repacked soil columns. Consequently, a common explanation for dissimilarities in microorganism transport in repacked columns and undisturbed soils is differences in water flow conditions. In particular, pathogen transport is expected to be enhanced when the bulk soil matrix is bypassed by rapid, preferential water flow. Field-scale experiments have frequently revealed that preferential pathways are a major contributor to the overall transport of microorganisms (Bales et al., 1989; Abu-Ashour et al., 1994; Jiang et al., 2010). Breakthrough concentrations for solutes and microbes in soils with preferential flow frequently exhibit physical nonequilibrium transport that is characterized by early arrival, concentration tailing, or multiple peaks (e.g., Pang, 2009; Sinreich and Flynn, 2011; Wang et al., 2013). Pathogens and/or subpopulations that survive for extended periods of time are especially susceptible to episodic preferential flow and transport events (de Roda Husman et al., 2009; Bradford et al., 2013).

Processes and conditions that lead to preferential flow have previously been reviewed in the literature (Hendrickx and Flury, 2001; Šimůnek et al., 2003; Jarvis, 2007). In brief, preferential water flow can occur as a result of: unstable flow behavior; dynamic capillary properties; macropores from decaying plant roots, burrowing earthworms, and animals; spatial variations in soil texture (layers and lenses) and soil structure; cracks in clayey soils; and fractured rocks. Surveys indicate that preferential flow occurs in most field soils (Flury et al., 1994; Hendrickx and Flury, 2001). The complexity of preferential flow processes presents an obstacle to accurate predictions of field-scale contaminant transport (Šimůnek et al., 2003).

A number of mathematical modeling approaches have been developed to simulate field-scale preferential water flow and transport. The classical uniform model (UM) describes water flow using either Richards' equation in the vadose zone or the Bousinesque equation for groundwater, and microbial transport using the advective–dispersion equation with first-order terms for retention, release, and decay (e.g., Harvey and Garabedian, 1991; Schijven et al., 1999; Zhang et al., 2001; Bradford et al., 2014). Subsurface heterogeneities and/or preferential pathways can be explicitly accounted for in the UM (e.g., Schelle et al., 2013; Wang et al., 2013), but this requires knowledge of the spatial variability in water flow and pathogen transport and fate parameters that is typically not available.

There is increasing evidence that the UM often cannot describe field observations, and a number of physical nonequilibrium flow and transport models have been developed to overcome this limitation (Gerke and van Genuchten, 1993; Vogel et al., 2000; Šimůnek et al., 2003; Gerke, 2006; Šimůnek and van Genuchten, 2008; Jarvis and Larsbo, 2012). The dual-permeability model (DPM) divides the soil into fast and slow flow domains at the representative elementary volume scale and solves separate flow and transport equations for each domain that include terms for the exchange of water and/or contaminants (Köhne et al., 2009a, 2009b; Šimůnek and van Genuchten, 2008). Preferential flow and transport in laboratory columns and at the plot or field scale are increasingly described using DPMs (e.g., Köhne et al., 2009a, 2009b; Wang et al., 2014).

Deterministic simulations for UMs and DPMs commonly consider only a single realization of flow and transport parameters. In this case, model output neglects uncertainty in flow and transport processes and parameters. Stochastic models have been developed to determine the mean and variance in flow and transport processes in the heterogeneous subsurface (e.g., Russo and Dagan, 2012; Fiori et al., 2015). The stochastic stream tube model (SSTM) is a simplified stochastic approach that describes field-scale variability in flow and/or other transport parameters using probability density functions (PDFs) in conjunction with a series of independent one-dimensional stream tubes (Toride et al., 1995; Maxwell et al., 2003; Bradford and Toride, 2007). However, conventional SSTMs do not allow for exchange between fast and slow flow domains and

have mainly been applied under steady-state flow conditions. The relative importance of these assumptions is expected to depend on the saturation conditions but has not yet been rigorously tested. In particular, exchange between fast and slow domains will be controlled by diffusion and dispersion under steady-state saturated flow conditions, whereas advection is expected to dominate exchange under variably saturated flow conditions. The use of the SSTM in conjunction with the dual-permeability description for individual stream tubes may potentially overcome this limitation but has only been the subject of preliminary investigation (Wang et al., 2014).

The transport distance to achieve the required amount of pathogen removal for safe drinking water production is referred to as the *setback distance*. Previous UMs, DPMs, and SSTMs have not always considered all relevant pathogen transport and fate processes such as flow velocity variations, irreversible and reversible retention, and solid- and liquid-phase decay that are needed to assess risk and safe setback distances. Furthermore, accurate quantification of field-scale flow and transport parameters remains a critical challenge for all of these models. Models that acceptably describe field data with the fewest number of model parameters are generally preferred because they are easier to calibrate and apply, especially for reactive contaminants like pathogens in poorly characterized subsurface environments. Approaches to predict pathogen transport and fate parameters are therefore critically important. One potential advantage of the SSTM is that the need to accurately characterize the spatial variation in the flow field is replaced by several parameters for the PDF that may potentially be determined from a conservative tracer test (Vanderborght et al., 2006). Some UMs have used CFT to predict values of k_{sw} in the field with varying degrees of success (e.g., Schijven et al., 1999; Zhang et al., 2001; Maxwell et al., 2003). To date, no DPMs or SSTMs have used CFT to predict microbial retention parameters.

A SSTM with velocity as the stochastic parameter is presented in this work that overcomes many of the above modeling limitations. In particular, the model includes additional pathogen and fate processes including filtration theory, unimodal or bimodal lognormal PDFs for the water velocity, and UM or DPM for individual stream tubes. The developed model was subsequently used to study the influence of various preferential flow factors on pathogen transport and fate, risk assessment, and the setback distance. Specific factors that were considered included: parameters from filtration theory (v, d_{50}, d_m, and α), the variance of the PDF, the PDF type (unimodal and bimodal lognormal distributions), the SSTM with UM or DPM in individual stream tubes, and the rate of exchange between fast and slow velocity regions.

Mathematical Models

Microorganism transport and retention was simulated in this work using four different model formulations, namely: (i) the UM; (ii) the DPM; (iii) the SSTM with the UM applied to individual stream tubes (SSTM-UM) using Darcy flux (q) from a unimodal or bimodal lognormal distribution; and (iv) the SSTM with the DPM applied to individual stream tubes (SSTM-DPM) with q from the same bimodal lognormal distribution for both permeability domains. Figure 1 provides conceptual illustrations of transport in each of these models as applied in this study. Steady-state, saturated water flow was assumed in all of these models to be consistent with the case of long-term ponded infiltration, as well as first-order microbial decay, release, and reversible and irreversible retention. The UM considers constant advective and dispersive transport in the downward direction. In this case, the microbe concentration is perfectly mixed in the direction perpendicular to water flow (Jury and Flühler, 1992). In contrast to the UM, the DPM allows for physical nonequilibrium transport. In particular, the DPM considers separate regions of fast and slow advective and dispersive transport in the downward direction and first-order diffusive and dispersive exchange between fast and slow regions. The SSTM-UM and SSTM-DPM describe field-scale transport using a series of independent stream tubes based on the UM and DPM, respectively, having separate values of q that were consistent with a field-scale probability density function. In contrast to the SSTM-UM, the SSTM-DPM allows diffusive and dispersive exchange between fast and slow velocity regions within an individual stream tube. Note that q is the stochastic parameter in the SSTM-UM and SSTM-DPM to reflect the spatial variability in the saturated hydraulic conductivity that is ubiquitous at the field scale. The mean and variance of the field-scale concentrations in the SSTM-UM and SSTM-DPM can be determined from the

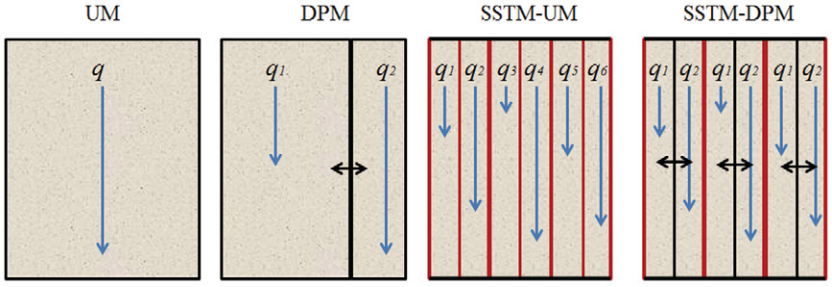

Fig. 1. Conceptual illustrations of microbe transport in the uniform model (UM), dual-permeability model (DPM), stochastic stream tube model (SSTM) with the UM applied to individual stream tubes (SSTM-UM) using Darcy flux (q) from a unimodal or bimodal lognormal distribution, and the SSTM with the DPM applied to individual stream tubes (SSTM-DPM) with q from the same bimodal lognormal distribution for both permeability domains. For convenience, only six stream tubes are shown for the SSTM-UM, whereas three stream tubes are given for the SSTM-DPM (outlined in red). In reality, both SSTM-UM and SSTM-DPM consider the full distribution of q.

local-scale stream tubes. All of these models assumed that the initial concentration in the simulation domain was zero, used a third-type boundary condition for pulse application at the inlet, and a concentration gradient of zero at a depth equal to infinity. Below, we briefly present the governing transport equations for each of these models.

Uniform Model

The aqueous-phase mass balance equation for microbes in the UM is written as follows when the volumetric water content and flux remain constant in time (steady-state water flow):

$$\frac{\partial C}{\partial t}=D\frac{\partial^2 C}{\partial z^2}-v\frac{\partial C}{\partial z}-(\mu_w+k_{sw})C+\frac{\rho_b k_{rs}}{\theta}S_r \quad [1]$$

where C [N L^{-3}; N and L denote the number of microbes and length, respectively] is the microbe concentration in the aqueous phase, S_r [N M^{-1}; M denotes units of mass] is the solid-phase concentration of reversibly retained microbes, t [T] is time, z [L] is depth, D is the hydrodynamic dispersion coefficient [L^2 T^{-1}], v is the average pore water velocity [L T^{-1}], ρ_b [M L^{-3}] is the soil bulk density, θ (dimensionless) is the volumetric water content, μ_w [T^{-1}] is the liquid-phase decay coefficient, and k_{sw} [T^{-1}] and k_{rs} [T^{-1}] are the microbe retention and release coefficients, respectively. The value of q is equal to the product of θ and v. The value of D is commonly approximated as the product of v and the dispersivity. The solid-phase mass balance equations for reversibly and irreversibly retained microbes are given as

$$\rho_b\frac{\partial S_r}{\partial t}=\theta F_{rev}k_{sw}C-\rho_b(\mu_s+k_{rs})S_r \quad [2]$$

$$\rho_b\frac{\partial S_i}{\partial t}=\theta(1-F_{rev})k_{sw}C-\rho_b\mu_s S_i \quad [3]$$

where S_i [N M^{-1}] is the solid-phase concentration of irreversibly retained microbes, μ_s [T^{-1}] is the solid-phase decay coefficient, and F_{rev} (dimensionless) is the fraction of reversibly retained microbes. The total local-scale solid-phase concentration of retained microbes, S [N M^{-1}], is equal to the sum of S_r and S_i. Toride et al. (1995) presented the analytic solutions to Eq. [1–3] that were used in this work.

Dual-Permeability Model

Separate aqueous- and solid-phase mass balance equations were used to describe transport and retention in fast (fracture) and slow (matrix) domains of the DPM (Leij and Bradford, 2013):

$$\frac{\partial C_1}{\partial t}=D_1\frac{\partial^2 C_1}{\partial z^2}-v_1\frac{\partial C_1}{\partial z}-(\mu_w+k_{sw1})C_1+\frac{\rho_b k_{rs1}}{\theta_1}S_{r1}-\Gamma(C_1-C_2) \quad [4]$$

$$\frac{\partial C_2}{\partial t}=D_2\frac{\partial^2 C_2}{\partial z^2}-v_2\frac{\partial C_2}{\partial z}-(\mu_w+k_{sw2})C_2+\frac{\rho_b k_{rs2}}{\theta_2}S_{r2}+\frac{\theta_1}{\theta_2}\Gamma(C_1-C_2) \quad [5]$$

$$\rho_b\frac{\partial S_{r1}}{\partial t}=\theta_1 F_{rev}k_{sw1}C_1-\rho_b(\mu_s+k_{rs1})S_{r1} \quad [6]$$

$$\rho_b\frac{\partial S_{i1}}{\partial t}=\theta_1(1-F_{rev})k_{sw1}C_1-\rho_b\mu_s S_{i1} \quad [7]$$

$$\rho_b\frac{\partial S_{r2}}{\partial t}=\theta_2 F_{rev}k_{sw2}C_2-\rho_b(\mu_s+k_{rs2})S_{r2} \quad [8]$$

$$\rho_b\frac{\partial S_{i2}}{\partial t}=\theta_2(1-F_{rev})k_{sw2}C_2-\rho_b\mu_s S_{i2} \quad [9]$$

where Γ [T^{-1}] is the mass transfer coefficient between fast and slow domains, and the subscripts 1 and 2 are used to denote the indicated parameters in the slow and fast domains, respectively. The total $S=S_1+S_2=S_{r1}+S_{i1}+S_{r2}+S_{i2}$, the total water content (θ) is $\theta=\theta_1+\theta_2$, and the total Darcy water velocity (q) is $q=q_1+q_2=\theta_1 v_1+\theta_1 v_2$. Alternatively, it is sometimes useful to write q_1 and q_2 in terms of the fraction of total water flow through the slow region, $\lambda_1=\theta_1 v_1/(\theta_1 v_1+\theta_1 v_2)$, as $q_1=\lambda_1 q$ and $q_2=(1-\lambda_1)q$. The total flux concentration is given as

$$C_F=\frac{q_1C_1+q_2C_2}{q_1+q_2} \quad [10]$$

Leij and Bradford (2013) presented the analytic solutions to Eq. [4–10] that were used in this work.

Stochastic Stream Tubes with Uniform Model

Average field-scale aqueous- and solid-phase microbial concentrations, $C_T(z,t)$ and $S_T(z,t)$, were obtained by integrating the contributions from individual UM stream tubes over the field-scale distribution of q as

$$C_T(z,t)=\frac{\langle qC(z,t;q)\rangle}{\langle q\rangle}=\frac{\int_0^\infty qf(q)C(z,t;q)\mathrm{d}q}{\int_0^\infty qf(q)\mathrm{d}q} \quad [11]$$

$$S_T(z,t)=\langle S(z,t;q)\rangle=\int_0^\infty f(q)S(z,t;q)\mathrm{d}q \quad [12]$$

where $C(z,t;q)$ and $S(z,t;q)$ are the aqueous- and solid-phase microbial concentrations, respectively, in an individual UM stream tube evaluated at a given value of q, and $f(q)$ is the field-scale probability density function for q. Integrals in Eq. [11] and [12] were evaluated numerically using the m-point Gauss–Chebyshev quadrature formula (e.g., Abramowitz and Stegun, 1972). The field-scale variance in microbe concentrations can also

be calculated using the SSTM. For example, the variance of $S_T(z,t)$ is given as $\langle S(z,t;q)^2\rangle - \langle S(z,t;q)\rangle^2$.

Field-scale variations in q were described using either unimodal or bimodal lognormal PDFs. The unimodal lognormal PDF is given as

$$f(q)=\frac{1}{q\sigma\sqrt{2\pi}}\exp\left[-\frac{(\ln(q)-\mu)^2}{2\sigma^2}\right] \quad [13]$$

where μ and σ are the mean and standard deviation of $\ln(q)$, respectively. Note that $\mu = \ln(\langle q\rangle) - 0.5\sigma^2$, where $\langle q\rangle$ is the ensemble average of q. The bimodal lognormal distribution may be used to describe more complex field-scale distributions of q as

$$f(q)=\frac{F_a}{q\sigma_a\sqrt{2\pi}}\exp\left\{-\frac{\left[\ln(q)-\mu_a\right]^2}{2\sigma_a^2}\right\} + \frac{(1-F_a)}{q\sigma_b\sqrt{2\pi}}\exp\left\{-\frac{\left[\ln(q)-\mu_b\right]^2}{2\sigma_b^2}\right\} \quad [14]$$

where subscripts a and b are included on μ, σ, and $\langle q\rangle$ to identify parameters associated with the two lognormal distributions, and F_a denotes the fraction of q that is assigned to lognormal distribution a.

Stochastic Stream Tubes with Dual-Permeability Model

The bimodal lognormal distribution of q (Eq. [14]) was used when using the SSTM-DPM. In this case, a constant value of λ_1 was used to determine $q_1 = \lambda_1 q$ and $q_2 = (1 - \lambda_1)q$ throughout the field. This simplification allowed the same bimodal lognormal distribution $f(q)$ to be used in both fast and slow domains of the DPM. Similar to the SSTM-UM, average field-scale values of $C_T(z,t)$ and $S_T(z,t)$ where obtained by integrating the contributions from individual DPM stream tubes over the field-scale distribution of q as

$$C_T(z,t)=\frac{\langle q_1C_1(z,t;q)+q_2C_2(z,t;q)\rangle}{\langle q\rangle} = \frac{\int_0^\infty f(q)\left[\lambda_1 qC_1(z,t;q)+(1-\lambda_1)qC_2(z,t;q)\right]dq}{\int_0^\infty qf(q)dq} \quad [15]$$

$$S_T(z,t)=\langle S_1(z,t;q)+S_2(z,t)\rangle = \int_0^\infty f(q)\left[S_1(z,t;q)+S_2(z,t;q)\right]dq \quad [16]$$

where aqueous-phase (C_1 and C_2) and solid-phase (S_1 and S_2) microbial concentrations in the slow and fast regions of an individual DPM stream tube were evaluated at a given value of q. Integrals and variances associated with the SSTM-DPM were determined in an analogous fashion to the SSTM-UM. In contrast to the SSTM-UM, the SSTM-DPM allows the role of exchange between slow and fast regions to be examined.

Numerical Experiments

The focus of this research was to numerically investigate the influence of field-scale velocity variations, including preferential flow, on pathogen transport and retention. Colloid filtration theory calculations and UM simulations were conducted to examine the influence of variations in q, d_{50}, and d_m. Simulations of the SSTM-UM with a unimodal lognormal PDF probed the roles of σ and α, whereas those with a bimodal lognormal PDF explored the influence of F_a. The DPM and SSTM-DPM simulations investigated the influence of Γ. Table 1 summarizes all of these simulations and associated model parameters.

Simulated microbe breakthrough curves (BTCs) and final retention profiles (RPs) are presented below for a four-pore-volume input pulse. The BTCs were plotted with the relative flux concentration (C/C_o for the UM, C_F/C_o for the DPM, and C_T/C_o for the SSTM-UM and SSTM-DPM; where C_o is the influent microbe concentration) on the vertical axis and pore volume on the horizontal axis, whereas semilog plots of the RPs are given with the normalized solid-phase microbe concentration (S/C_o for the UM and DPM, and S_T/C_o for the SSTM-UM and SSTM-DPM) on the vertical log axis and depth on the horizontal axis. The BTCs and RPs are given at a depth of 10 cm and after eight pore volumes to facilitate the visualization of microbe concentrations. The number of pore volumes was determined as $\langle q\rangle t/(\theta L_D)$, where L_D is the length of the considered simulation domain. A constant value of dispersivity was assumed in all simulations equal to $0.1L_D$. Values of θ and ρ_b were also constants equal to 0.36 and 1.70 g cm^{-3}, respectively, to be consistent with typical values in sand (e.g., Schaap et al., 2001).

The mathematical equations above included processes of liquid- and solid-phase decay, release, and reversible and irreversible retention for completeness. Liquid- and solid-phase decay parameters and F_{irr} were set to zero ($F_{rev} = 1$) in numerical experiments to better study the processes of pathogen transport and reversible retention at the field scale. Pathogen release under steady-state conditions is a slow, diffusion-controlled process, and the release rate coefficient is typically several orders of magnitude smaller than the retention rate coefficient (Ryan and Elimelech, 1996). Very limited research has therefore been directed to predicting the release rate coefficient under steady-state conditions (Johnson et al., 1995; Harter et al., 2000). Consequently, values of k_{rs}, k_{rs1}, and k_{rs2} were set to low values of 0.001 min^{-1} that are typical for packed column studies (Bradford et al., 2016).

Colloid filtration theory was used to estimate the influence of various physicochemical conditions on k_{sw} for the UM and SSTM-UM as (Yao et al., 1971)

$$k_{sw}=\frac{3(1-\theta)}{2d_{50}}\eta\alpha v \quad [17]$$

Table 1. A summary of all model parameters used in the numerical experiments in Fig. 2 through 8.

Figure no.	Simulation parameters
Fig. 2	Colloid filtration theory (CFT) predictions using Eq. [17] and the correlation equation of Messina et al. (2015). In Fig. 2a, the sticking efficiency $\alpha = 1$, the median grain size (d_{50}) = 360 μm, the microbe density was 1.08 g cm^{-3}, the microbe size (d_m) ranges from 1 to 20,000 nm, and the Darcy flux q = 0.001, 0.001, 0.01, 0.1, 1, and 10 cm min^{-1}. In Fig. 2b, the value of $\alpha = 1$, the microbe density was 1.08 g cm^{-3}, d_m ranges from 1 to 20,000 nm, q = 0.1 cm min^{-1}, and d_{50} = 50, 100, 200, 400, 800, and 1000 μm.
Fig. 3–8	Constant model information and parameters for Fig. 3–8 include the following: steady-state, saturated downward flow with unit hydraulic gradient; input pulse duration = four pore volumes; total simulation duration = eight pore volumes; the domain length L_D = 10 cm; volumetric water content θ = 0.36; bulk density (ρ_b) = 1.7 g cm^{-3}; microbe density is 1.08 g cm^{-3}; dispersivity = 0.1L_D; the fraction of reversibly retained microbes (F_{rev}) = 1 and irreversibly retained microbes (F_{irr}) = 0; liquid-phase decay coefficient (μ_l) = 0 min^{-1} and the solid-phase decay coefficient (μ_s) = 0 min^{-1}; microbe retention rate coefficients k_{sw}, k_{sw1}, and k_{sw2} were determined using CFT (Eq. [17]) and the correlation equation of Messina et al. (2015); correlation between q and d_{50} using Eq. [18] and uniformity coefficient U_i = 4; and microbe release rate coefficients $k_{rs} = k_{rs1} = k_{rs2}$ = 0.001 min^{-1}. Breakthrough curves are given at a distance of 10 cm, and retention profiles are given after eight pore volumes. Other specific model parameters are provided below.
Fig. 3	Uniform model (UM) simulations with $\alpha = 0.05$, d_m = 1000 nm, and q = 0.05, 0.1, 0.25, 0.5, and 1 cm min^{-1}.
Fig. 4	Dual-permeability model (DPM) simulations with $\alpha = 0$ (Fig. 4a) and $\alpha = 0.1$ (Fig. 4b), d_m = 1000 nm, $\theta_1 = \theta_2 = 0.5\theta = 0.18$, q = 0.1 cm min^{-1}, the fraction of total water flow through the slow region (λ_1) = 0.2 such that flow through the slow region q_1 = 0.02 cm min^{-1} and flow through the fast region q_2 = 0.08 cm min^{-1}, and the mass transfer coefficient between the fast and slow domains (Γ) = 0.0001, 0.001, 0.01, and 0.1 min^{-1}.
Fig. 5	Stochastic stream tube model SSTM-UM simulations when $\alpha = 0.0$, d_m = 1500 nm, and q is described using a unimodal lognormal distribution with $\langle q \rangle$ = 0.05 cm min^{-1} and σ = 0.1, 1, and 2.
Fig. 6	SSTM-UM simulations with α = 0.01, 0.05, and 0.1, d_m = 1500 nm, and q described using a unimodal lognormal distribution with $\langle q \rangle$ = 0.05 cm min^{-1} and $\sigma = 1$.
Fig. 7	SSTM-UM simulations with $\alpha = 0.1$, d_m = 1000 nm, and q described using the bimodal lognormal distribution with $\langle q_a \rangle$ = 0.1 cm min^{-1}, $\langle q_b \rangle$ = 2.0 cm min^{-1}, $\sigma_a = 0.1$, $\sigma_b = 0.5$, and the fraction of q assigned to distribution a (F_a) = 0.9, 0.925, 0.95, 0.975, and 0.999.
Fig. 8	SSTM-DPM simulations with $\alpha = 0.1$, d_m = 1000 nm, $\theta_1 = \theta_2 = 0.5\theta = 0.18$, $\lambda_1 = 0.2$, and Γ = 0.0001, 0.001, 0.01, and 0.1 min^{-1}, and q is described using the bimodal lognormal distribution with $\langle q_a \rangle$ = 0.1 cm min^{-1}, $\langle q_b \rangle$ = 2.0 cm min^{-1}, $\sigma_a = 0.1$, $\sigma_b = 0.5$, and $F_a = 0.975$.

The correlation equation of Messina et al. (2015) was used in this work to predict η as a nonlinear function of q, d_{50}, and d_m when using a microbe density of 1.08 g cm^{-3}. Note that Eq. [17] depends on the interconnected parameters q (or v) and d_{50}. Values of q were therefore related to grain size distribution parameters using Darcy's Law with a unit hydraulic gradient to be consistent with steady-state, saturated downward flow (Fig. 1). In particular, the saturated hydraulic conductivity (K_s, L T^{-1}) was estimated from the representative soil grain size using the Kozeny–Carman equation (Bear, 1972) as

$$K_s = \frac{\rho_w g}{\chi_w}\left[\frac{d_{10}^2}{180}\frac{\theta^3}{(1-\theta)^2}\right] \qquad [18]$$

where ρ_w [M L^{-3}] is the density of water, χ_w [M L^{-1} T^{-1}] is the dynamic viscosity of water, and g [L T^{-2}] is the acceleration due to gravity. In this study, the representative soil grain size was taken to be d_{10} [L] (Lemke et al., 2004), i.e., where 10% of the soil mass is finer than d_{10}. Note that $d_{50} \approx d_{10}U_i$, where U_i is the uniformity coefficient that was taken to be 4. The use of Eq. [18] in this manner allowed q to be related to d_{50} in CFT calculations.

Colloid filtration theory originally assumed that α in Eq. [17] was controlled by the adhesive interaction (e.g., Elimelech et al., 1998). In reality, α depends on hydrodynamic and adhesive forces and torques that act on microbes near the solid–water interface (SWI), as well as fluctuations in molecular kinetic energy that produces a random Brownian force (Cushing and Lawler, 1998). The hydrodynamic force and torque that act on a microbe adjacent to the SWI depend on the microbe size, the water velocity, and the pore-space geometry (grain size distribution, grain–grain contacts, and microscopic roughness) (Bradford et al., 2011). The adhesive force and its torque depend on the solution- and solid-phase chemistries, the microbe size, shape, and deformation, and nanoscale roughness and chemical heterogeneity on both the SWI and the microbe (Bradford and Torkzaban, 2015). Due to these many complexities, the value of α was set to representative values during the simulations discussed below. A value of $\alpha = 0$ is for a nonreactive microbe, whereas larger values indicate greater retention.

The value of q in individual streams tubes of the SSTM-UM and SSTM-DPM were determined from PDFs (Eq. [13] or [14]). Parameters of these PDFs can be determined by inverse optimization to heterogeneous field-scale BTCs of a conservative tracer. An example application of the SSTM-UM to describe transport of reactive solutes in heterogeneous soils was given in Vanderborght et al. (2006). However, hypothetical values of PDF parameters were used in our numerical experiments (Table 1). Similarly, values of q_1 and q_2 in the DPM and SSTM-DPM were determined using the constraint $q = q_1 + q_2 = \lambda_1 q + (1 - \lambda_1)q$ with $\lambda_1 = 0.2$. Dual-permeability models typically assume that only a small fraction of the porous medium is associated with fast flow such that $\theta_2 << \theta_1$. To facilitate comparison of the SSTM-UM and SSTM-DPM, the values of θ_1 and θ_2 were set to 0.5θ such that $\theta = \theta_1 + \theta_2$ and the slow and fast regions had the same size. Values of k_{sw1} and k_{sw2} in the DPM and SSTM-DPM were also estimated using CFT. In

particular, values of v and q in Eq. [17] and [18] were replaced by v_1 and $q_1\theta/\theta_1$, respectively, when determining k_{sw1}. In this study, $q_1\theta/\theta_1$ upscales q_1 from θ_1 to θ for CFT calculations. The value k_{sw2} was determined in a similar manner to k_{sw1}.

Results and Discussion

Uniform Model

Colloid filtration theory was used to predict the complex dependency of k_{sw} on d_m, d_{50}, and q. Figures 2a and 2b present plots of the predicted influence of d_m on k_{sw} for several different q (Fig. 2a) and d_{50} (Fig. 2b) values when $\alpha = 1$. The value of d_{50} equals 360 μm in Fig. 2a, and q equals 0.1 cm min^{-1} in Fig. 2b. Note that k_{sw} achieved a minimum when d_m ranged between 955 and 1700 nm depending on q and d_{50}, and this reflects the optimum microbe size for transport (the lowest amount of mass transfer to the SWI is a worst-case scenario for pathogen transport). The value of k_{sw} also increases in a nonlinear manner with q, with a greater velocity dependence predicted for smaller and larger microbes (Fig. 2). The dominant mechanism of microbe mass transfer to the SWI occurs via sedimentation and interception for larger d_m and q, whereas the relative importance of diffusion increases for smaller d_m and q. In addition, the value of k_{sw} also increases with decreasing d_{50} (Fig. 2b). The CFT predictions in Fig. 2 are consistent with published literature (e.g., Tufenkji and Elimelech, 2004; Messina et al., 2015) and are presented to aid the interpretation of subsequent modeling results.

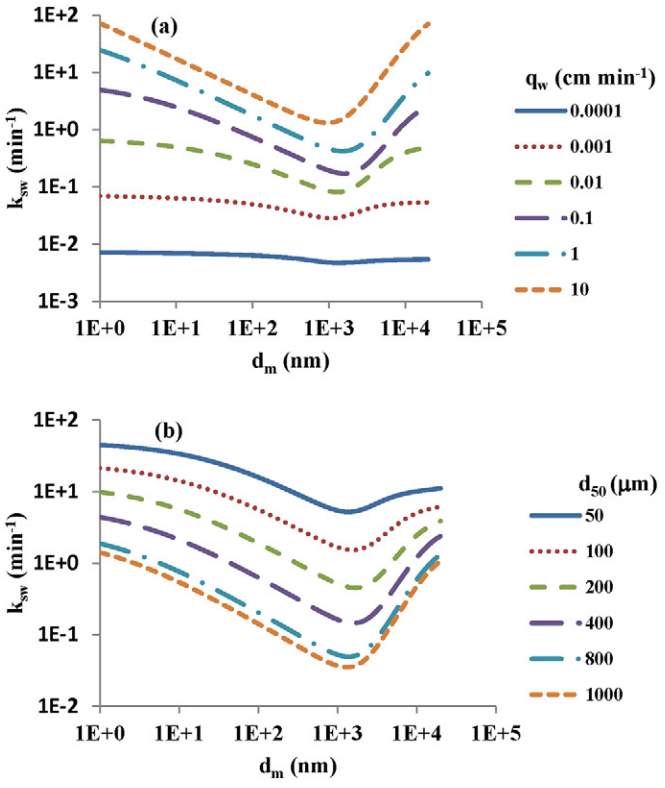

Fig. 2. Plots of the predicted influence of microbe diameter (d_m) on the retention rate coefficient k_{sw} for several different values of (a) the Darcy velocity q for a median grain size (d_{50}) of 360 μm and (b) d_{50} with a q of 0.1 cm min^{-1} when using filtration theory and the correlation equation of Messina et al. (2015) with sticking efficiency $\alpha = 1$. See Table 1 for all parameter values.

Uniform model simulations were conducted to illustrate the influence of q on pathogen transport and retention. In this case, the value of q was correlated with d_{50} using Eq. [18]. Figures 3a and 3b present illustrative examples of the predicted influence of q (0.05, 0.1, 0.25, 0.5, and 1 cm min^{-1}) on BTCs and RPs, respectively, when $\alpha = 0.05$ and $d_m = 1000$ nm. Other model parameters are given in Table 1. The value of q has a strong influence on BTCs and RPs because microbe retention depends on both the advection-controlled residence time and the velocity dependency of k_{sw}. Greater microbe retention occurs with decreasing q because of an increase in the residence time, even though k_{sw} decreases with decreasing q (Fig. 2a). However, this velocity dependency will also depend on the microbe size because of differences in k_{sw} with d_m (Fig. 2). Many previous experimental and modeling studies have examined the influence of q on microbe transport and retention, and the simulation results shown in Fig. 3 are generally consistent with this published literature (e.g., Meinders et al., 1995; Hendry

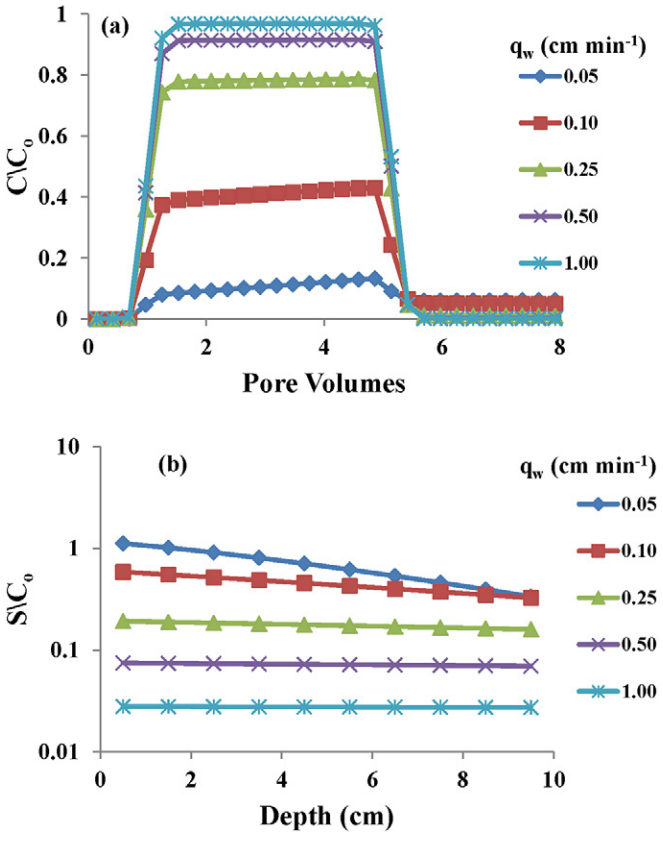

Fig. 3. Predicted (a) breakthrough curves and (b) retention profiles for the uniform model with colloid filtration theory when sticking efficiency $\alpha = 0.05$, microbe diameter $d_m = 1000$ nm, and Darcy velocity $q = 0.01$, 0.05, 0.1, 0.25, 0.5, and 1 cm min^{-1}. The median grain size d_{50} was determined from q using Eq. [18]. See Table 1 for all parameter values.

et al., 1999; Schijven and Hassanizadeh, 2000). However, the explicit coupling between q and d_{50} in CFT predictions has typically not been considered. Figure 3 was therefore needed to help interpret the DPM and SSTM-UM results.

Dual-Permeability Model

Figures 4a and 4b present BTCs from the DPM for different values of Γ (0.0001, 0.001, 0.01, and 0.1 min^{-1}) for $\alpha = 0$ (Fig. 4a) and $\alpha = 0.1$ (Fig. 4b). Model parameters included $d_m = 1000$ nm, $\theta = 0.36$, $\theta_1 = 0.18$, $\theta_2 = 0.18$, $q = 0.1$ cm min^{-1}, $q_1 = 0.02$ cm min^{-1}, and $q_2 = 0.08$ cm min^{-1}, as well as others given in Table 1. In contrast to the UM, the DPM exhibits physical nonequilibrium, with breakthrough occurring much earlier than one pore volume and extensive concentration tailing in some cases. However, the apparent amount of physical nonequilibrium depends on values of Γ and α. In particular, physical nonequilibrium transport is always greatest when Γ is smallest. The BTCs become more similar as Γ increases when there is no retention ($\alpha = 0$), such that the apparent influence of preferential flow is diminished and the BTC approaches that of a UM. Conversely, increased mixing (higher Γ) when $\alpha = 0.1$ produces greater amounts of retention in the low-velocity region (Fig. 3), and differences in BTCs therefore become greater. The DPM has commonly been used for simulating preferential flow and transport in undisturbed columns and at the plot or field scale, and the results shown in Fig. 4 are consistent with this literature (e.g., Gerke and van Genuchten, 1993; Šimůnek et al., 2003; Šimůnek and van Genuchten, 2008; Köhne et al., 2009a, 2009b; Wang et al., 2014). However, CFT has not previously been incorporated into the DPM, and Fig. 4 is needed to interpret the SSTM-DPM simulations.

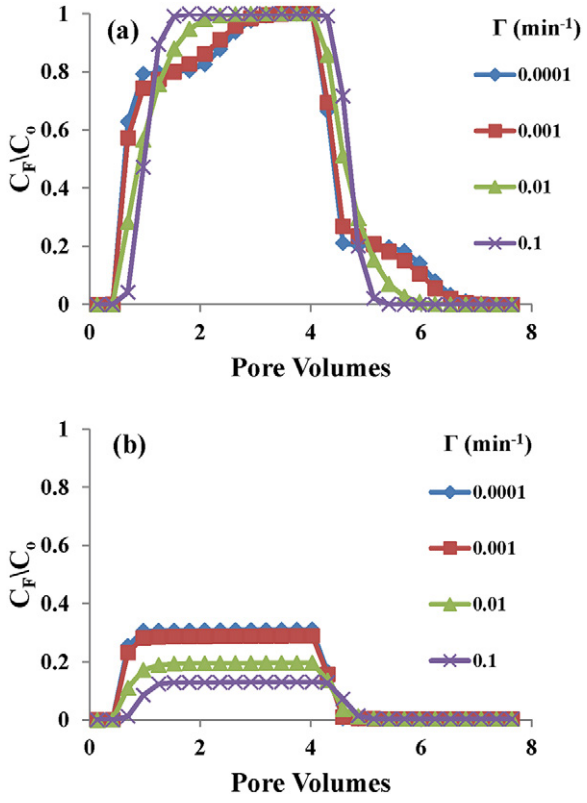

Fig. 4. Predicted breakthrough curves for the dual-permeability model with colloid filtration theory when sticking efficiency α is (a) 0 and (b) 0.1 and the mass transfer coefficient between the fast and slow domains (Γ) = 0.0001, 0.001, 0.01, and 0.1 min^{-1}. Other model parameters included microbe diameter $d_m = 1000$ nm, Darcy velocity $q = 0.1$ cm min^{-1}, velocity through the slow domain $q_1 = 0.02$ cm min^{-1}, velocity through the fast domain $q_2 = 0.08$ cm min^{-1}, volumetric water content $\theta = 0.36$, $\theta_1 = 0.18$, and $\theta_2 = 0.18$. See Table 1 for all parameter values.

Stochastic Stream Tubes with Uniform Model

Figure 5a presents the predicted BTCs when $d_m = 1500$ nm, $\alpha = 0.0$, and q was described using a unimodal lognormal distribution with $\langle q \rangle = 0.05$ cm min^{-1} and $\sigma = 0.1$, 1, and 2. Other model parameters are given in Table 1. Values of $\sigma = 0.1$, 1, and 2 were chosen based on the available literature (Woodbury and Sudicky, 1991; Jussel et al., 1994; Bradford et al., 1998) to represent low, intermediate, and high levels of heterogeneity in q, respectively. The corresponding variance in C_T/C_o is shown in Fig. 5b. In this case, the microbe transport behavior is consistent with a conservative tracer because $\alpha = 0.0$. Note that increasing σ produces greater amounts of physical nonequilibrium and a larger variance

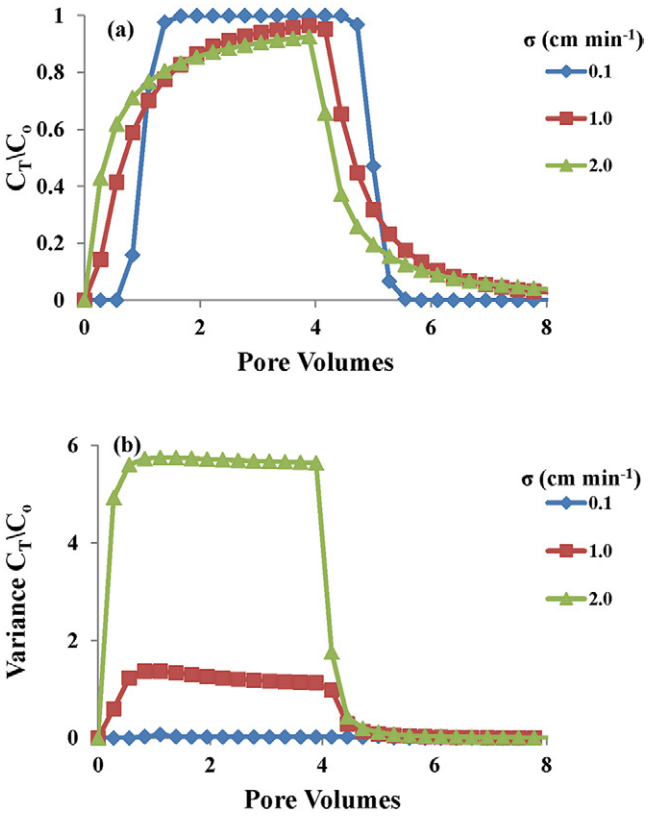

Fig. 5. The (a) mean and (b) variance of predicted breakthrough curves for the uniform model applied to individual stream tubes (SSTM-UM) when the microbe diameter (d_m) is 1500 nm, the sticking efficiency (α) is 0.0, and the Darcy velocity (q) is described with a unimodal lognormal distribution with $\langle q \rangle = 0.05$ cm min^{-1} and $\sigma = 0.1$, 1, and 2. See Table 1 for all parameter values.

in C_T/C_o. Breakthrough occurs earlier with increasing σ because of the presence of higher velocity stream tubes. The concentration tailing is controlled by the amount of lower velocity stream tubes.

Figures 6a and 6b present predicted BTCs and RPs when d_m = 1500 nm, α = 0.01, 0.05, and 0.1, and q was described using a unimodal lognormal distribution with $<q>$ = 0.05 cm min^{-1} and σ = 1. Other model parameters are given in Table 1. Note that small values of α have a large influence on the shape of BTCs and RPs. In particular, increasing α produces a greater amount of retention, as expected, but also increases the relative importance of high-velocity stream tubes. For example, BTCs in Fig. 6a are increasingly dominated by earlier breakthrough that is controlled by high-velocity stream tubes when α increases. The low-concentration tailing is mainly eliminated with increasing α because greater residence times and retention occur in the low-velocity stream tubes (Fig. 3). The RP profiles also become more hyper-exponential with increasing α for a similar reason. The BTCs for individual stream tubes tend to separate with increasing time and distance due to differences in advection and pathogen removal. Slower stream tubes will eventually be depleted of pathogens, and the ultimate transport potential will be controlled by the highest velocity stream tubes with lower retention. Note that previous

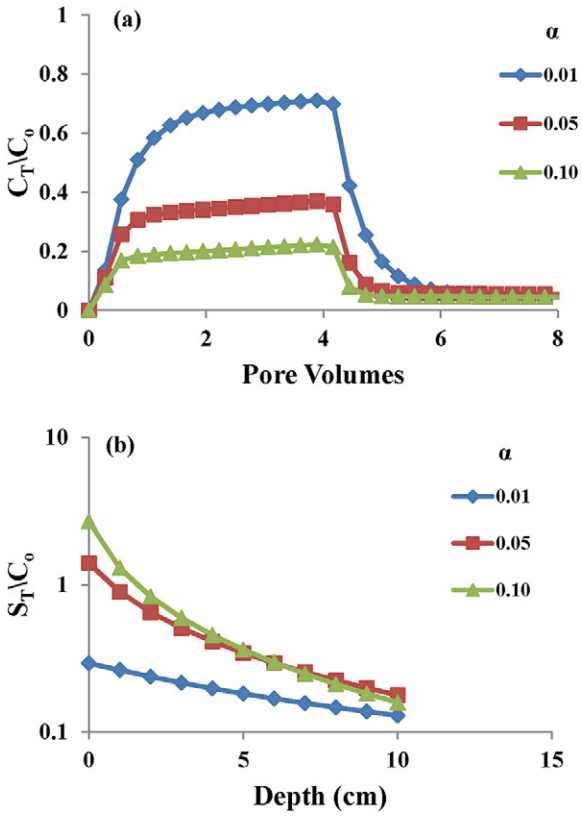

Fig. 6. Predicted (a) breakthrough curves and (b) retention profiles for the uniform model applied to individual stream tubes (SSTM-UM) when the microbe diameter (d_m) is 1500 nm, the sticking efficiency (α) is 0.01, 0.05, and 0.1, and the Darcy velocity (q) is described using a unimodal lognormal distribution with $<q>$ = 0.05 cm min^{-1} and σ = 1. See Table 1 for all parameter values.

application of the SSTM-UM to describe microbe transport has not used CFT in conjunction with Eq. [18] (Maxwell et al., 2003; Bradford and Toride, 2007), so the predicted influence of q on retention was only partially examined.

The parameter k_{sw} is proportional to α (Eq. [17]). Consequently, other factors that increase pathogen retention will influence BTCs and RPs in a similar manner to increasing α (Fig. 6). In particular, Fig. 2 and 3 indicate that pathogen retention increases with smaller and larger values of d_m (Fig. 2) and decreasing q (Fig. 3). Consequently, smaller (e.g., viruses) and larger (e.g., *Cryptosporidium* oocysts) pathogens are expected to exhibit an even larger sensitivity to changes in α than that shown in Fig. 6. In addition, the influence of physical nonequilibrium (early breakthrough and tailing) increases with σ (Fig. 5), and this also produces greater amounts of retention and even more hyper-exponential RPs when α > 0 (Bradford and Toride, 2007). Interestingly, a variety of colloids (microbes, latex microspheres, and nanoparticles) have been commonly observed at the column scale to exhibit a hyper-exponential RP shape that is sensitive to the physicochemical conditions (Bradford et al., 2014). The above information indicates that this may at least be partially explained by differences in the pore-scale velocity distribution that cause greater retention in lower than higher velocity regions.

A unimodal lognormal distribution (Eq. [13]) may be inadequate to describe natural velocity distributions in the field. The bimodal lognormal distribution (Eq. [14]) provides increased flexibility to describe more complex velocity distributions that are typical of preferential flow. Figures 7a and 7b present illustrative examples of predicted BTCs and RPs when d_m = 1000 nm and α = 0.1, and the field-scale velocity is described using the bimodal lognormal distribution with $<q_a>$ = 0.1 cm min^{-1}, $<q_b>$ = 2.0 cm min^{-1}, σ_a = 0.1, σ_b = 0.5, and F_a = 0.9, 0.925, 0.95, 0.975, and 0.999. Other model parameters are given in Table 1. Some of the BTCs exhibit multiple plateaus after breakthrough due to the presence of the bimodal velocity distribution. Decreasing F_a produces greater amounts of preferential transport with earlier breakthrough time, increasing breakthrough concentrations, and a corresponding decrease in the amount of retention. Preferential transport is associated with smaller amounts of retention (Fig. 3). Consequently, retention profiles were mainly controlled by low-velocity steam tubes. No published SSTM-UM studies have used the bimodal lognormal PDF for q.

Stochastic Stream Tubes with Dual-Permeability Model

Figure 8 presents the mean (Fig. 8a) and variance (Fig. 8b) in simulated BTCs when using the SSTM-DPM when Γ = 0.0001, 0.001, 0.01, and 0.1 min^{-1}. Similar bimodal lognormal distribution parameters were used as in Fig. 7 ($<q_a>$ = 0.1 cm min^{-1}, $<q_b>$ = 2.0 cm min^{-1}, σ_a = 0.1, σ_b = 0.5, and F_a = 0.975), and d_m = 1000 nm, α = 0.1, λ_1 = 0.2, and $\theta_1 = \theta_2 = 0.5\theta = 0.18$. Other

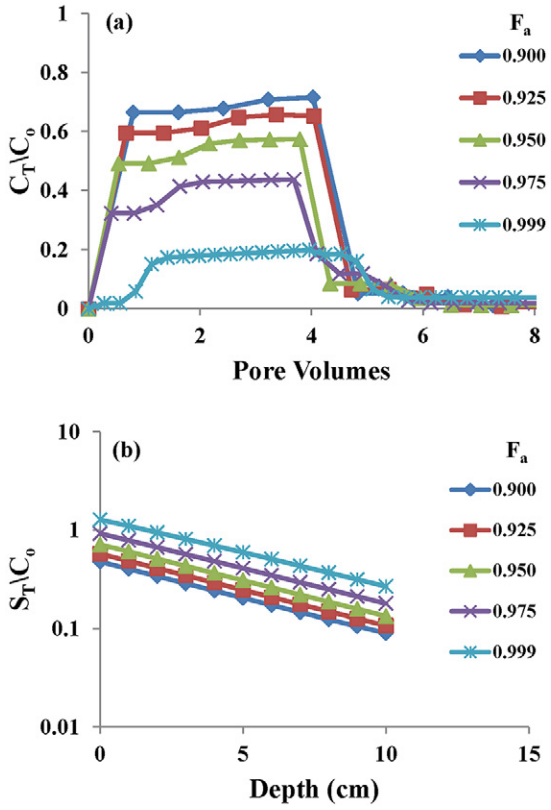

Fig. 7. Predicted (a) breakthrough curves and (b) retention profiles for the uniform model applied to individual stream tubes (SSTM-UM) when the microbe diameter (d_m) is 1000 nm, the sticking efficiency (α) is 0.1, and the Darcy velocity (q) is described using the bimodal lognormal distribution with $<q_a>$ = 0.1 cm min^{-1}, $<q_b>$ = 2.0 cm min^{-1}, σ_a = 0.1, σ_b = 0.5, and the fraction of q assigned to lognormal distribution a (F_a) = 0.9, 0.925, 0.95, 0.975, and 1. See Table 1 for all parameter values.

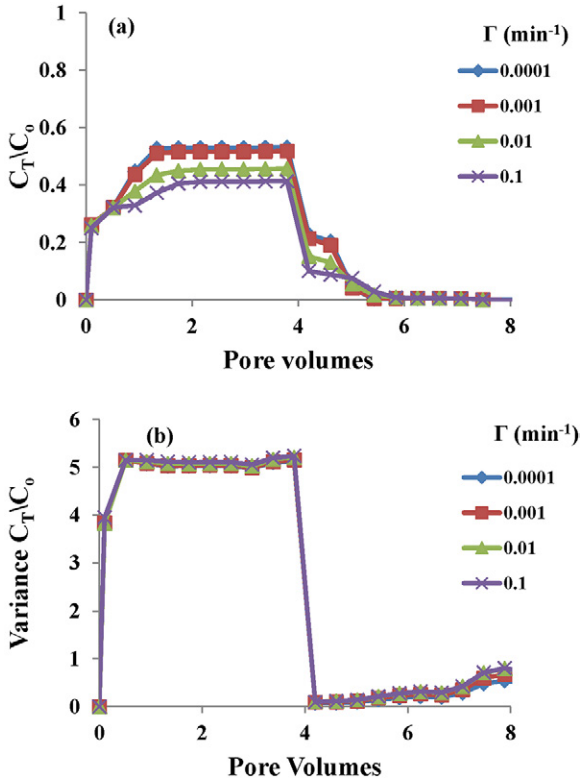

Fig. 8. The (a) mean and (b) variance of predicted breakthrough curves for the dual-permeability model applied to individual stream tubes (SSTM-DPM) when the sticking efficiency α = 0.1 and the mass transfer coefficient between the fast and slow domains (Γ) = 0.0001, 0.001, 0.01, and 0.1 min^{-1}. Other model parameters included microbe diameter (d_m) = 1000 nm; volumetric water contents overall (θ) = 0.36, in the slow domain (θ_1) = 0.18, and the fast domain (θ_2) = 0.18; the fraction of total water flow through the slow region (λ_1) = 0.2; mean Darcy velocity assigned to lognormal distribution a $<q_a>$ = 0.1 cm min^{-1} and lognormal distribution b ($<q_b>$) = 2 cm min^{-1}; σ_a = 0.1 and σ_b = 0.5; and the fraction of q assigned to lognormal distribution a (F_a) = 0.975. See Table 1 for all parameter values.

model parameters are given in Table 1. Similar to the DPM (Fig. 4b), increasing Γ produces greater amounts of retention due to enhanced mixing and retention in lower velocity regions. In contrast to the DPM (Fig. 4b) and SSTM-UM (Fig. 7a), greater amounts of physical nonequilibrium are possible with the SSTM-DPM because of the use of both a bimodal lognormal distribution for q and high- and low-velocity regions within a stream tube. Consequently, the SSTM-DPM with low Γ provides a worst-case scenario for determining pathogen transport and risk assessment. However, comparison of Fig. 7a and 8a reveals that the SSTM-UM and SSTM-DPM approach each other as Γ increases and enhances the mixing within a stream tube. The variance in C_T was relatively insensitive to the value of Γ (Fig. 8b), suggesting that it was primarily controlled by mean breakthrough concentrations (Fig. 8a) and parameters of the bimodal lognormal distribution. Wang et al. (2014) provided illustrative preliminary simulations for the SSTM-DPM approach that considered only heterogeneity in high-velocity regions embedded in a uniform matrix material and did not consider CFT or Eq. [18]. No other studies have been published with the SSTM-DPM.

Risk Assessment and Setback Distances

The World Health Organization has recommended a health-based target for tap water consumption of not more than one infection per 10,000 people per year, which is consistent with a maximum pathogen concentration on the order of 10^{-6} N L^{-1} (World Health Organization, 2011). In contrast, typical concentrations of pathogenic *Cryptosporidium* and of enteroviruses in the effluent of large wastewater treatment plants are on the order of 100 N L^{-1} (e.g., Schijven et al., 2015). Hence, effluent from wastewater treatment plants needs an additional 8 $\log_{10}$ (100 million-fold) reduction in pathogen concentration before it can serve as drinking water. Soil passage during riverbank filtration, sand filtration, and natural and managed aquifer recharge is frequently relied on to achieve this reduction in pathogen concentration. Runoff water from urban and agricultural settings can have much higher pathogen concentrations than treated wastewater effluents (e.g., Bradford et al., 2013), and it may therefore need greater treatment by soil passage to meet health guidelines. Consistent with treated wastewater effluent, an 8 $\log_{10}$ reduction

in pathogen concentration was assumed to determine the setback distance in this work.

Figure 9 illustrates the predicted influence of q on the setback distance for a continuous input of *Cryptosporidium parvum* oocyst concentration when using the UM and measured model parameters (Bradford et al., 2016) of d_m = 4300 nm, α = 0.32, F_{rev} = 0.58, k_{rs} = 0.0011 min^{-1}, dispersivity = 0.07 cm, porosity = 0.47, and assuming no decay. The setback distance increases in nearly a linear fashion with q. In addition to q, the required setback distance will depend on the pathogen type, the required concentration reduction, as well as differences in model parameters.

Figure 9 presents the setback distance in terms of the UM but it is also valid for individual stream tubes in the SSTM-UM. A distribution of water velocities at the field scale will influence risk assessment by producing a variance in the pathogen concentration (Fig. 5b and 8b). Risk assessment is strongly influenced by the distribution tails that produce a low probability of higher concentrations. Figure 9 illustrates this point by showing plots of the cumulative density function for q when it is lognormally distributed with $<q>$ = 0.2 cm min^{-1} and σ = 0.1, 0.5, 1.0, and 2.0. Note that the setback distance based on $<q>$ = 0.2 cm min^{-1} does not account for the large influence of high-velocity regions on risk. Much larger setback distances are needed to ensure adequate removal in the highest velocity stream tubes. This is especially true when σ increases. For example, the maximum setback distance is equal to about 1 m when σ = 0.1, whereas it is 151 m when σ = 2.0.

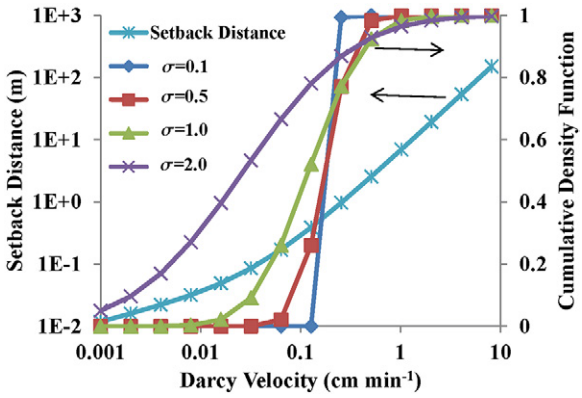

Fig. 9. The predicted influence of the Darcy velocity q on the setback distance to achieve an 8 $\log_{10}$ reduction in *Cryptosporidium parvum* oocyst concentration when using the uniform model and measured values (Bradford et al., 2016) of microbe diameter d_m = 4300 nm, sticking efficiency α = 0.32, the fraction of reversible retained microbes F_{rev} = 0.58, microbe release rate coefficient k_{rs} = 0.0011 min^{-1}, dispersivity = 0.07 cm, porosity = 0.47, and assuming no decay. The cumulative unimodal lognormal probability density functions for q are also shown when $<q>$ = 0.2 cm min^{-1} and σ = 0.1, 0.5, 1.0, and 2.0.

Summary and Conclusions

The SSTM was extended to better study pathogen transport and fate at the field scale. In particular, unimodal or bimodal PDFs for the velocity distribution were considered, and individual stream tubes were modified to include UM or DPM transport models with additional processes (e.g., filtration theory and reversible and irreversible retention). Simulation results demonstrated that pathogen transport and fate, risk assessment, and setback distances are highly dependent on the field-scale velocity distribution. A distribution of water velocities in the SSTM causes greater retention in low-velocity stream tubes because of higher residence times, and transport therefore mainly occurs in high-velocity stream tubes. Increasing the spread of the velocity distribution produces more physical nonequilibrium transport that is characterized by breakthrough earlier than one pore volume, concentration tailing, and non-exponential retention profile shapes. These physical nonequilibrium effects are coupled with k_{sw} and q, with diminished concentration tailing and hyper-exponential retention profiles occurring for higher values of k_{sw} and lower q. The DPM results demonstrated that exchange between high- and low-velocity regions enhanced pathogen retention and the relative importance of high-velocity regions on pathogen transport. In contrast to the UM and DPM, the SSTM approach allowed the mean and variance in pathogen concentrations to be determined. This concentration variance impacts risk assessment and the predicted setback (transport) distance to treat water. A worst-case transport scenario occurred with the SSTM-DPM, and predicted setback distances were controlled by the highest velocity regions of the distribution. However, the SSTM-UM approaches the SSTM-DPM when the exchange rate between low- and high-velocity domains is high.

Acknowledgments

This research was supported by the USDA–ARS National Program 211.

References

Abramowitz, M., and I.A. Stegun. 1972. Handbook of mathematical functions. 10th printing with corrections. Dover, Mineola, NY.

Abu-Ashour, J., D.M. Joy, H. Lee, H.R. Whiteley, and S. Zelin. 1994. Transport of microorganisms through soil. Water Air Soil Pollut. 75:141–158. doi:10.1007/BF01100406

Arnaud, E., A. Best, B.L. Parker, R. Aravena, and K. Dunfield. 2015. Transport of *Escherichia coli* through a thick vadose zone. J. Environ. Qual. 44:1424–1434. doi:10.2134/jeq2015.02.0067

Bales, R.C., C.P. Gerba, G.H. Grondin, and S.L. Jensen. 1989. Bacteriophage transport in sandy soil and fractured tuff. Appl. Environ. Microbiol. 55:2061–2067.

Bear, J. 1972. Dynamics of fluids in porous media. American Elsevier, New York.

Borchardt, M.A., K.R. Bradbury, E.C. Alexander, R.J. Kolberg, S.C. Alexander, J.R. Archer, et al. 2011. Norovirus outbreak caused by a new septic system in a dolomite aquifer. Ground Water 49:85–97. doi:10.1111/j.1745-6584.2010.00686.x

Borchardt, M.A., K.R. Bradbury, M.B. Gotkowitz, J.A. Cherry, and B.L. Parker. 2007. Human enteric viruses in groundwater from a confined bedrock aquifer. Environ. Sci. Technol. 41:6606–6612. doi:10.1021/es071110+

Bradford, S.A., L.M. Abriola, and K.M. Rathfelder. 1998. Flow and entrapment of dense nonaqueous phase liquids in physically and chemically heterogeneous aquifer formations. Adv. Water Resour. 22:117–132. doi:10.1016/S0309-1708(98)00005-0

Bradford, S.A., H. Kim, B. Headd, and S. Torkzaban. 2016. Evaluating the transport of *Bacillus subtilis* spores as a potential surrogate for *Cryp-*

tosporidium parvum oocysts. Environ. Sci. Technol. 50:1295–1303. doi:10.1021/acs.est.5b05296

Bradford, S.A., V.L. Morales, W. Zhang, R.W. Harvey, A.I. Packman, A. Mohanram, and C. Welty. 2013. Transport and fate of microbial pathogens in agricultural settings. Crit. Rev. Environ. Sci. Technol. 43:775–893. doi:10.1080/10643389.2012.710449

Bradford, S.A., and N. Toride. 2007. A stochastic model for colloid transport and deposition. J. Environ. Qual. 36:1346–1356. doi:10.2134/jeq2007.0004

Bradford, S.A., and S. Torkzaban. 2015. Determining parameters and mechanisms of colloid retention and release in porous media. Langmuir 31:12096–12105. doi:10.1021/acs.langmuir.5b03080

Bradford, S.A., S. Torkzaban, and A. Wiegmann. 2011. Pore-scale simulations to determine the applied hydrodynamic torque and colloid immobilization. Vadose Zone J. 10:252–261. doi:10.2136/vzj2010.0064

Bradford, S.A., Y. Wang, H. Kim, S. Torkzaban, and J. Šimůnek. 2014. Modeling microorganism transport and survival in the subsurface. J. Environ. Qual. 43:421–440. doi:10.2134/jeq2013.05.0212

Craun, G.F., J.M. Brunkard, J.S. Yoder, V.A. Roberts, J. Carpenter, T. Wade, et al. 2010. Causes of outbreaks associated with drinking water in the United States from 1971 to 2006. Clin. Microbiol. Rev. 23:507–528. doi:10.1128/CMR.00077-09

Cushing, R.S., and D.F. Lawler. 1998. Depth filtration: Fundamental investigation through three-dimensional trajectory analysis. Environ. Sci. Technol. 32:3793–3801. doi:10.1021/es9707567

de Roda Husman, A.M., W.J. Lodder, S.A. Rutjes, J.F. Schijven, and P.F.M. Teunis. 2009. Long-term inactivation study of three enteroviruses in artificial surface and groundwaters, using PCR and cell culture. Appl. Environ. Microbiol. 75:1050–1057. doi:10.1128/AEM.01750-08

Elimelech, M., J. Gregory, X. Jia, and R.A. Williams. 1998. Particle deposition and aggregation measurement, modeling, and simulation. Butterworth-Heinemann, Woburn, MA.

Embrey, S.S., and D.L. Runkle. 2006. Microbial quality of the nation's groundwater resources, 1993–2004. Sci. Invest. Rep. 2006-5290. USGS, Reston, VA.

Fiori, A., A. Bellin, V. Cvetkovic, F.P.J. de Barros, and G. Dagan. 2015. Stochastic modeling of solute transport in aquifers: From heterogeneity characterization to risk analysis. Water Resour. Res. 51:6622–6648. doi:10.1002/2015WR017388

Flury, M., H. Flühler, W.A. Jury, and J. Leuenberger. 1994. Susceptibility of soils to preferential flow of water: A field study. Water Resour. Res. 30:1945–1954. doi:10.1029/94WR00871

Flynn, R.M., G. Mallèn, M. Engel, A. Ahmed, and P. Rossi. 2015. Characterizing aquifer heterogeneity using bacterial and bacteriophage tracers. J. Environ. Qual. 44:1448–1458. doi:10.2134/jeq2015.02.0117

Foppen, J.W.A., and J.F. Schijven. 2006. Evaluation of data from the literature on the transport and survival of *Escherichia coli* and thermotolerant coliforms in aquifers under saturated conditions. Water Res. 40:401–426. doi:10.1016/j.watres.2005.11.018

Gerke, H.H. 2006. Preferential flow descriptions for structured soils. J. Plant Nutr. Soil Sci. 169:382–400. doi:10.1002/jpln.200521955

Gerke, H.H., and M.Th. van Genuchten. 1993. A dual-porosity model for simulating the preferential movement of water and solutes in structured porous media. Water Resour. Res. 29:305–319. doi:10.1029/92WR02339

Ginn, T.R., B.D. Wood, K.E. Nelson, T.D. Scheibe, E.M. Murphy, and T.P. Clement. 2002. Processes in microbial transport in the natural subsurface. Adv. Water Resour. 25:1017–1042. doi:10.1016/S0309-1708(02)00046-5

Gupta, V., W.P. Johnson, P. Shafieian, H. Ryu, A. Alum, M. Abbaszadegan, et al. 2009. Riverbank filtration: Comparison of pilot scale transport with theory. Environ. Sci. Technol. 43:669–676. doi:10.1021/es8016396

Harter, T., S. Wagner, and E.R. Atwill. 2000. Colloid transport and filtration of *Cryptosporidium parvum* in sandy soils and aquifer sediments. Environ. Sci. Technol. 34:62–70. doi:10.1021/es990132w

Harvey, R.W., and S.P. Garabedian. 1991. Use of colloid filtration theory in modeling movement of bacteria through a contaminated sandy aquifer. Environ. Sci. Technol. 25:178–185. doi:10.1021/es00013a021

Harvey, R.W., and H. Harms. 2002. Transport of microorganisms in the terrestrial subsurface: In situ and laboratory methods. In: C.J. Hurst et al., editors, Manual of environmental microbiology. ASM Press, Washington, DC. p. 753–776.

Hendrickx, J.M., and M. Flury. 2001. Uniform and preferential flow mechanisms in the vadose zone. In: Conceptual models of flow and transport in the fractured vadose zone. Natl. Acad. Press, Washington, DC. p.. 149–187.

Hendry, M.J., J.R. Lawrence, and P. Maloszewski. 1999. Effects of velocity on the transport of two bacteria through saturated sand. Ground Water 37:103–112. doi:10.1111/j.1745-6584.1999.tb00963.x

Jarvis, N.J. 2007. A review of non-equilibrium water flow and solute transport in soil macropores: Principles, controlling factors and consequences for water quality. Eur. J. Soil Sci. 58:523–546. doi:10.1111/j.1365-2389.2007.00915.x

Jarvis, N., and M. Larsbo. 2012. MACRO(v 5.2): Model use, calibration, and validation. Trans. ASABE 55:1413–1423. doi:10.13031/2013.42251

Jiang, S., L.P. Pang, G.D. Buchan, J. Šimůnek, M.J. Noonan, and M.E. Close. 2010. Modeling water flow and bacterial transport in undisturbed lysimeters under irrigations of dairy shed effluent and water using HYDRUS-1D. Water Res. 44:1050–1061. doi:10.1016/j.watres.2009.08.039

Jin, Y., and M. Flury. 2002. Fate and transport of viruses in porous media. Adv. Agron. 77:39–102. doi:10.1016/S0065-2113(02)77013-2

Johnson, W.P., K.A. Blue, B.E. Logan, and R.G. Arnold. 1995. Modeling bacterial detachment during transport through porous media as a residence-time-dependent process. Water Resour. Res. 31:2649–2658. doi:10.1029/95WR02311

Jury, W.A., and H. Flühler. 1992. Transport of chemicals through soil: Mechanisms, models, and field applications. Adv. Agron. 47:141–201. doi:10.1016/S0065-2113(08)60490-3

Jussel, P., F. Stauffer, and T. Dracos. 1994. Transport modeling in heterogeneous aquifers: 1. Statistical description and numerical generation of gravel deposits. Water Resour. Res. 30:1803–1817. doi:10.1029/94WR00162

Kazner, C., T. Wintgens, and P. Dillon. 2012. Water reclamation technologies for safe managed aquifer recharge. IWA Publ., London.

Kim, H.N., S.L. Walker, and S.A. Bradford. 2010. Coupled factors influencing the transport and retention of *Cryptosporidium parvum* oocysts in saturated porous media. Water Res. 44:1213–1223. doi:10.1016/j.watres.2009.09.041

Köhne, J.M., S. Köhne, and J. Šimůnek. 2009a. A review of model applications for structured soils: A. Water flow and tracer transport. J. Contam. Hydrol. 104:4–35. doi:10.1016/j.jconhyd.2008.10.002

Köhne, J.M., S. Köhne, and J. Šimůnek. 2009b. A review of model applications for structured soils: B. Pesticide transport. J. Contam. Hydrol. 104:36–60. doi:10.1016/j.jconhyd.2008.10.003

LeBlanc, D.R., S.P. Garabedian, K.M. Hess, L.W. Gelhar, R.D. Quadri, K.G. Stollenwerk, and W.W. Wood. 1991. Large-scale natural gradient tracer test in sand and gravel, Cape Cod, Massachusetts: 1. Experimental design and observed tracer movement. Water Resour. Res. 27:895–910. doi:10.1029/91WR00241

Leij, F.J., and S.A. Bradford. 2013. Colloid transport in dual-permeability media. J. Contam. Hydrol. 150:65–76. doi:10.1016/j.jconhyd.2013.03.010

Lemke, L.D., L.M. Abriola, and P. Goovaerts. 2004. Dense nonaqueous phase liquid (DNAPL) source zone characterization: Influence of hydraulic property correlation on predictions of DNAPL infiltration and entrapment. Water Resour. Res. 40:W01511. doi:10.1029/2003WR001980

Li, X., E.R. Atwill, E. Antaki, O. Applegate, B. Bergamaschi, R.F. Bond, et al. 2015. Fecal indicator and pathogenic bacteria and their antibiotic resistance in alluvial groundwater of an irrigated agricultural region with dairies. J. Environ. Qual. 44:1435–1447. doi:10.2134/jeq2015.03.0139

Maxwell, R.M., C. Welty, and A.F. Tompson. 2003. Streamline-based simulation of virus transport resulting from long term artificial recharge in a heterogeneous aquifer. Adv. Water Resour. 26:1075–1096. doi:10.1016/S0309-1708(03)00074-5

Meinders, J.M., H.C. van der Mei, and H.J. Busscher. 1995. Deposition efficiency and reversibility of bacterial adhesion under flow. J. Colloid Interface Sci. 176:329–341. doi:10.1006/jcis.1995.9960

Messina, F., D.L. Marchisio, and R. Sethi. 2015. An extended and total flux normalized correlation equation for predicting single-collector efficiency. J. Colloid Interface Sci. 446:185–193. doi:10.1016/j.jcis.2015.01.024

Mualem, Y. 1976. A new model for predicting the hydraulic conductivity of unsaturated porous media. Water Resour. Res. 12:513–522. doi:10.1029/WR012i003p00513

Pang, L. 2009. Microbial removal rates in subsurface media estimated from published studies of field experiments and large intact soil cores. J. Environ. Qual. 38:1531–1559. doi:10.2134/jeq2008.0379

Ray, C., G. Melin, and R.B. Linsky. 2003. Riverbank filtration: Improving source-water quality. Springer, Dordrecht, the Netherlands.

Rockhold, M.L., R.R. Yarwood, and J.S. Selker. 2004. Coupled microbial and transport processes in soils. Vadose Zone J. 3:368–383. doi:10.2136/vzj2004.0368

Russo, D., and G. Dagan, editors. 2012. Water flow and solute transport in soils: Developments and applications in memoriam Eshel Bresler (1930–1991). Adv. Ser. Agric Sci. 20. Springer, Berlin.

Ryan, J.N., and M. Elimelech. 1996. Colloid mobilization and transport in groundwater. Colloid Surf. A 107:1–56. doi:10.1016/0927-7757(95)03384-X

Schaap, M.G., F.J. Leij, and M.Th. van Genuchten. 2001. ROSETTA: A computer program for estimating soil hydraulic parameters with hierarchical pedotransfer functions. J. Hydrol. 251:163–176. doi:10.1016/S0022-1694(01)00466-8

Schelle, H., W. Durner, S. Schlüter, H.-J. Vogel, and J. Vanderborght. 2013. Virtual soils: Moisture measurements and their interpretation by inverse modeling. Vadose Zone J. 12(3). doi:10.2136/vzj2012.0168

Schijven, J., J. Derx, A.M. de Roda Husman, A.P. Blaschke, and A.H. Farnleitner. 2015. QMRAcatch: Microbial quality simulation of water resources including infection risk assessment. J. Environ. Qual. 44:1491–1502. doi:10.2134/jeq2015.01.0048

Schijven, J.K., and S.M. Hassanizadeh. 2000. Removal of viruses by soil passage: Overview of modeling, processes, and parameters. Crit. Rev. Environ. Sci. Technol. 30:49–127. doi:10.1080/10643380091184174

Schijven, J.F., W. Hoogenboezem, M. Hassanizadeh, and J.H. Peters. 1999. Modeling removal of bacteriophages MS2 and PRD1 by dune recharge at Castricum, Netherlands. Water Resour. Res. 35:1101–1111. doi:10.1029/1998WR900108

Schijven, J.F., J.H.C. Mülschlegel, S.M. Hassanizadeh, P.F.M. Teunis, and A.M. de Roda Husman. 2006. Determination of protection zones for Dutch groundwater wells against virus contamination: Uncertainty and sensitivity analysis. J. Water Health 4:297–312. doi:10.2166/wh.2006.012

Schijven, J.F., P.F. Teunis, S.A. Rutjes, M. Bouwknegt, and A.M. de Roda Husman. 2011. QMRAspot: A tool for quantitative microbial risk assessment from surface water to potable water. Water Res. 45:5564–5576. doi:10.1016/j.watres.2011.08.024

Šimůnek, J., N.J. Jarvis, M.Th. van Genuchten, and A. Gardenas. 2003. Review and comparison of models for describing non-equilibrium and preferential flow and transport in the vadose zone. J. Hydrol. 272:14–35. doi:10.1016/S0022-1694(02)00252-4

Šimůnek, J., and M.Th. van Genuchten. 2008. Modeling nonequilibrium flow and transport processes using HYDRUS. Vadose Zone J. 7:782–797. doi:10.2136/vzj2007.0074

Sinreich, M., and R. Flynn. 2011. Comparative tracing experiments to investigate epikarst structural and compositional heterogeneity. Speleogenesis Evol. Karst Aquifers 10:60–67.

Steele, M., and J. Odumeru. 2004. Irrigation water as source of foodborne pathogens on fruit and vegetables. J. Food Prot. 67:2839–2849. doi:10.4315/0362-028X-67.12.2839

Taylor, R., A. Cronin, S. Pedley, J. Barker, and T. Atkinson. 2004. The implications of groundwater velocity variations on microbial transport and wellhead protection: Review of field evidence. FEMS Microbiol. Ecol. 49:17–26. doi:10.1016/j.femsec.2004.02.018

Toride, N., F.J. Leij, and M.Th. van Genuchten. 1995. The CXTFIT code for estimating transport parameters from laboratory or filed tracer experiments. US Salinity Lab., Riverside, CA.

Tufenkji, N., and M. Elimelech. 2004. Correlation equation for predicting single-collector efficiency in physicochemical filtration in saturated porous media. Environ. Sci. Technol. 38:529–536. doi:10.1021/es034049r

Unc, A., and M.J. Goss. 2004. Transport of bacteria from manure and protection of water resources. Appl. Soil Ecol. 25:1–18. doi:10.1016/j.apsoil.2003.08.007

UN World Water Assessment Program. 2015. World water development report 2015: Water for a sustainable world. UNESCO, Paris. http://www.unesco.org/new/en/loginarea/natural-sciences/environment/water/wwap/wwdr/2015-water-for-a-sustainable-world/.

Vanderborght, J., R. Kasteel, and H. Vereecken. 2006. Stochastic continuum transport equations for field-scale solute transport. Vadose Zone J. 5:184–203. doi:10.2136/vzj2005.0024

van Genuchten, M.Th. 1980. A closed-form equation for predicting the hydraulic conductivity of unsaturated soils. Soil Sci. Soc. Am. J. 44:892–898. doi:10.2136/sssaj1980.03615995004400050002x

Vogel, T., H.H. Gerke, R. Zhang, and M.Th. van Genuchten. 2000. Modeling flow and transport in a two-dimensional dual-permeability system with spatially variable hydraulic properties. J. Hydrol. 238:78–89. doi:10.1016/S0022-1694(00)00327-9

Wang, Y., S.A. Bradford, and J. Šimůnek. 2013. Transport and fate of microorganisms in soils with preferential flow under different solution chemistry conditions. Water Resour. Res. 49:2424–2436. doi:10.1002/wrcr.20174

Wang, Y., S.A. Bradford, and J. Šimůnek. 2014. Estimation and upscaling of dual-permeability model parameters for the transport of *E. coli* D21g in soils with preferential flow. J. Contam. Hydrol. 159:57–66. doi:10.1016/j.jconhyd.2014.01.009

Woodbury, A.D., and E.A. Sudicky. 1991. The geostatistical characteristics of the Borden aquifer. Water Resour. Res. 27:533–546. doi:10.1029/90WR02545

World Health Organization. 2011. Guidelines for drinking-water quality. 4th ed. WHO, Geneva, Switzerland.

Yao, K.-M., M.T. Habibian, and C.R. O'Melia. 1971. Water and waste water filtration: Concepts and applications. Environ. Sci. Technol. 5:1105–1112. doi:10.1021/es60058a005

Zhang, P., W.P. Johnson, T.D. Scheibe, K.H. Choi, F.C. Dobbs, and B.J. Mailloux. 2001. Extended tailing of bacteria following breakthrough at the Narrow Channel Focus Area, Oyster, Virginia. Water Resour. Res. 37:2687–2698. doi:10.1029/2000WR000151